Research article

Landobasa Y. M. Tobing, Michał Wasiak, Dao Hua Zhang*, Weijun Fan* and Tomasz Czyszanowski*

Nearly total optical transmission of linearly polarized light through transparent electrode composed of GaSb monolithic high-contrast grating integrated with gold

https://doi.org/10.1515/nanoph-2021-0286
Received June 5, 2021; accepted September 10, 2021; published online September 22, 2021

Abstract: Achieving high transmission of light through a highly conductive structure implemented on a semiconductor remains a challenge in optoelectronics as the transmission is inevitably deteriorated by absorption and Fresnel reflection. There have been numerous efforts to design structures with near-unity transmission, yet they are typically constrained by a trade-off between conductivity and optical transmission. To address this problem, we propose and demonstrate a transmission mechanism enabled by a monolithic GaSb subwavelength grating integrated with Au stripes (metalMHCG). Near-unity transmission of polarized light is achieved by inducing low-quality factor resonance in the air gaps between the semiconductor grating stripes, which eliminates light absorption and reflection by the metal. Our numerical simulation shows 97% transmission of transverse magnetic polarized light and sheet resistance of 2.2 ΩSq^{-1}. The metalMHCG structure was realized via multiple nanopatterning and dry etching, with the largest transmission yet reported of ~90% at a wavelength of 4.5 μm and above 75% transmission in the wavelength range from 4 to 10 μm and sheet resistance at the level of 26 ΩSq^{-1}. High optical transmission is readily achievable using any high refractive index materials employed in optoelectronics. The design of the metalMHCG is applicable in a wide electromagnetic spectrum from near ultraviolet to infrared.

Keywords: monolithic high contrast grating; subwavelength grating; transparent electrode.

1 Introduction

Electrically conductive and transparent layers implemented at the semiconductor surface are in high demand for interactive electronics [1–4], concentrator photovoltaics [5–8], light-emitting diodes (LEDs) [9], and surface-emitting lasers (SELs) [10, 11]. Simultaneously addressing the requirements of low sheet resistance and high optical transmission remains a scientific and technological challenge. The most common solution for both electrical conductivity and optical transparency is to deposit a layer of indium tin oxide (ITO). However, the conductivity of the ITO layer comes at the expense of light absorption, which imposes a trade-off between high electrical conductivity and high optical transmission. For this reason, ITO layers are typically employed for low-current applications. Moreover, due to free-carrier absorption in the near- and far-infrared spectrum [12], the use of ITO as transparent electrodes is limited to the visible spectrum. An alternative solution is offered by meta-structures, in the form of periodic metal grids or irregular metal nanowire networks [13]. However, because the pitch of such periodic structures, or the average distance between their nanowires, is larger than the wavelength, their thickness is minimized to reduce interaction with the electromagnetic field, which inevitably contributes to

***Corresponding authors: Dao Hua Zhang and Weijun Fan**, School of Electrical & Electronic Engineering, Nanyang Technological University, 50 Nanyang Avenue, Singapore, 639798, Singapore, E-mail: edhzhang@ntu.edu.sg (D.H. Zhang), ewjfan@ntu.edu.sg (W. Fan); and **Tomasz Czyszanowski**, Photonics Group, Institute of Physics, Lodz University of Technology, ul. Wolczanska 219, Łódź, 90-924, Poland, E-mail: tomasz.czyszanowski@p.lodz.pl. https://orcid.org/0000-0002-0283-5074 (T. Czyszanowski)
Landobasa Y. M. Tobing, School of Electrical & Electronic Engineering, Nanyang Technological University, 50 Nanyang Avenue, Singapore, 639798, Singapore
Michał Wasiak, Photonics Group, Institute of Physics, Lodz University of Technology, ul. Wolczanska 219, Łódź, 90-924, Poland

absorption, reflection, scattering, and diffraction. Other approaches include, for example, the implementation of thin carbon-based layers [14].

All these solutions are susceptible to Fresnel reflection, which occurs at the smooth interface between materials of different refractive indices [15]. As described by Fresnel equations, light transmission can be reduced by 20–40%, assuming a typical refractive index contrast between the semiconductor and air. Fresnel reflection can be eliminated by antireflection coatings, yet these are typically nonconductive dielectrics, which deteriorate current injection into the semiconductor. Another approach that enables total optical transmission is the guided-mode resonance effect, which can be realized by dielectric subwavelength gratings. The high-quality factor of the resonance enables high transmission in a narrow spectral range providing effective spectral filtering [16–18]. However, a reduction in both the parasitic absorption of the conductive layer and Fresnel reflection in the broad spectral range can be achieved using a thin metal layer patterned with subwavelength periodic arrangements of one-dimensional (1D) slits or two-dimensional (2D) holes facilitated by propagating and localized surface plasmon (SP) modes [19]. This type of transmission, based on the extraordinary optical transmission (EOT) mechanism [20–28], results from resonant excitation of SPs. When the grating period is in the deep subwavelength range, 90% of the transverse magnetic (TM) polarized light (the magnetic component of the electromagnetic field parallel to the walls of the slits) can be transmitted through the 1D metal grating in the infrared spectrum. However, this EOT mechanism is rather suppressed in the visible and near-infrared (NIR) spectrum due to the increased optical loss of plasmonic metals in the visible and NIR spectrum. As a result, transmission through a 1D grating becomes smaller than the Fresnel transmission through the plane interface between the semiconductor and air [29].

Another mechanism responsible for reduced transmission is the creation of SPs at the metal-semiconductor interface, where the creation of SPs increases light reflection and absorption at the expense of transmission [30, 31]. In such a configuration, the transmission of transverse electric (TE) polarization is drastically reduced. Indeed, the observed counteracting phenomena in TE and TM transmissions through a 1D metal grating play an ambivalent role in the mechanism of transmission through 2D metal structures, resulting in comparable or lower transmission compared to the transmission through an ITO layer [32].

Using numerical analysis [33], we proposed a semiconductor deep-subwavelength monolithic high-contrast grating integrated with metal (metalMHCG) to address the above problems. The metalMHCG design consists of metal stripes implemented on top of semiconductor grating stripes. The incident plane wave of TM polarization couples to low-quality factor cavity resonance (CRs), enabling broadband transmission. The localization of CR in the air gaps between the semiconductor stripes impedes the formation of SPs at the interfaces between the metal and semiconductor stripes. This effect almost completely eliminates metal absorption, which is responsible for the deterioration of transmittance in structures with metal gratings on semiconductor substrates [29]. The metalMHCG can serve in low electrical power applications in which current is transported in the plane of the metal stripes but mostly in numerous high power applications as top transparent electrode enabling current flow to or from the semiconductor as for example in vertical-cavity surface-emitting lasers, surface-emitting lasers, light emitting diodes, and photodetectors. In all those applications, the direction of the current flow and the light propagation is the same, which enforces the use of ring contacts together with current confining regions [34] that deteriorate the efficiency of the devices due to the current crowding effect [35]. We expect that the metalMHCG can serve as a highly conductive transparent electrode in those devices enabling fully vertical current flow and exceptional optical properties that are examined in this paper.

In this paper, we report the first fabricated semiconductor deep-subwavelength monolithic high-contrast grating integrated with metal (metalMHCG). The configuration is transparent to TM polarization and is designed for maximal transmission at a wavelength of 4.5 μm. The structure is fabricated from GaSb, with gold stripes deposited on top of a GaSb grating. In what follows, we show by numerical calculations using the plane-wave reflection transformation method [33, 36] that a carefully designed metalMHCG configuration enables nearly 100% optical power transmittance. This is in line with the high transmission observed experimentally for the metalMHCG structure in the same configuration.

2 Results

The metalMHCG used in the calculations consists of a semi-infinite, monolithic undoped semiconductor substrate with etched stripes on the surface and a semi-infinite air superstrate. Gold stripes 50 nm thick are deposited on top of the semiconductor stripes (Figure 1). In the calculations, we consider a single period of the grating with periodic boundary conditions, which elongate the grating to infinity

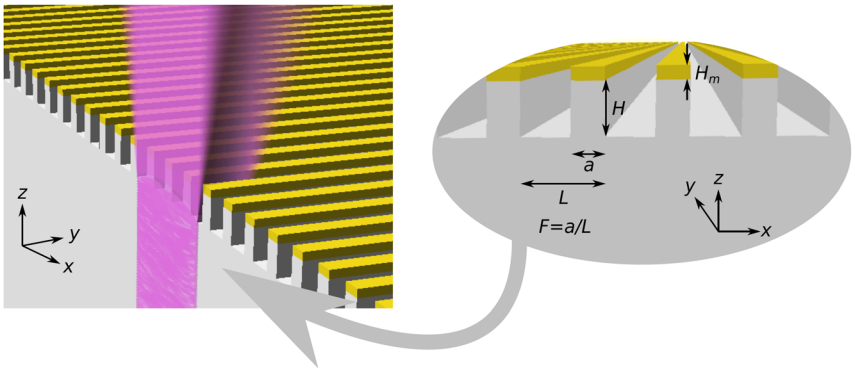

Figure 1: MetalMHCG composed of semiconductor bars implemented on a substrate of the same material (in gray) with metal stripes (yellow) implemented on top of the semiconductor bars. The geometrical parameters of the metalMHCG are defined in the figure.

in the lateral direction. The parameters of the metalMHCG are as follows: L – period of the grating, set to 0.8 μm; a – width of the grating stripe, set to 0.5 μm; H – height of the semiconductor stripe. In the numerical analysis presented below, H is a variable. The values for L and a are optimized with respect to the maximal transmission for a wavelength of around 4.5 μm, according to the procedure presented in [33]. The refractive indices of the semiconductor grating n_s and metal n_m are given by dispersion characteristics based on [37, 38].

Calculated transmission mappings of a metalMHCG illuminated by TM and TE polarization at normal incidence are presented in Figure 2(a) and (b), respectively. At least one grating mode exists in the subwavelength region ($\lambda < L\, n_s$). Interference between the incident plane wave and the grating mode(s) induces a typical pattern of low and high transmissions through the grating [39], which enables narrowband transmissions with maximal values of ~50%. In the deep subwavelength regime ($\lambda > L\, n_s$), the pattern of transmission bands resembles the Fabry–Perot (FP) mechanism, suggesting that instead of coupling to the grating modes, the incident plane wave creates a low-quality factor etalon between the two interfaces of the metalMHCG [37] one at the interface of the grating with the semiconductor surface and the other at the interface of the grating with air.

In the case of TM polarization, Fresnel reflection is eliminated when the incident plane wave couples to the CR, which is located in the air gaps between the stripes (Figure 2(c)). In the case of TE polarization, the plane wave couples to the CR in the high refractive index stripes (Figure 2(d)). The metal at the top of the grating stripe thus prohibits the transmission of TE polarization throughout the deep subwavelength regime (Figure 2(b)).

The configuration with metal stripes only (H = 0) enables more than 65% transmission for λ > 10 μm (see Figure S1 in Supplementary Materials illustrating measured and calculated transmissions). Increasing the transmission in this configuration to 90% requires careful design of the gold stripes. In particular, it requires a very short grating period with respect to the wavelength, given by the condition $L/\lambda > 0.05$. Moreover, transmission is an oscillating-like and decaying function of the gold height [30]. By contrast, the metalMHCG allows for greater flexibility in the choice of the grating parameters, particularly the height of the metal stripes which can be varied smoothly in the range $H_m/\lambda < 0.7$, enabling transmission above 95%. The grating period can be as large as $L/\lambda = 0.18$ [33], which significantly relaxes the fabrication requirements. Based on the results shown in Figure 2(a), we demonstrated this metalMHCG concept experimentally, by investigating the transmission of metalMHCG with 50 nm thick Au stripes implemented on top of a GaSb grating.

The metalMHCG was fabricated by a combination of multistep patterning and dry etching (as described in detail in Supplementary materials S1), where the gold grating and the MHCG structures are to be fabricated with precise alignments. Owing to the serial nature of electron beam lithography, in which the patterns consist of write-fields that are stitched together, alignment errors are likely to occur and propagate from one write field to another. To avoid this error, the metalMHCG pattern was realized within a single write field, with alignment markers designed to have a Vernier-type shape for more accurate alignment. Using this strategy, a metalMHCG structure with good alignment was achieved, as illustrated in the false-colored scanning electron microscope (SEM) images in Figure 3(a) and (b). The MHCG was made 10 μm longer than the metal stripes to facilitate inspection of their alignment at the edges of the sample. The alignment quality between the patterns is generally evaluated via the overlaid vernier markers (Figure 3(c)), where the first marker (associated with the gold grating) and second marker (associated with the MHCG) are close to the ideal layout depicted in the inset.

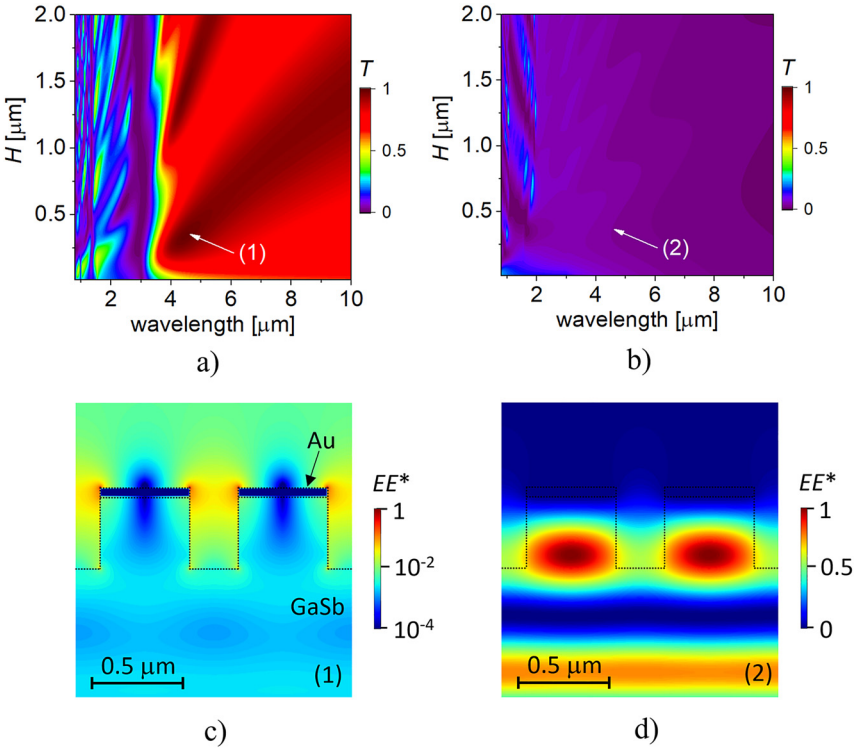

Figure 2: Calculated maps of transmittance (T) for metalMHCGs in the domain of wavelength and grating height (H) for $a = 0.5$ μm and $L = 0.8$ μm with TM (a) and TE (b) polarization. Numbers (1) and (2) indicate the metalMHCG configurations with $H = 0.38$ μm and corresponding light distributions illustrated in (c) and (d), respectively. Distributions of optical field intensity within a metalMHCG illuminated by TM (c) and TE (d) polarization. Transmission of TM and TE polarizations for configuration indicated by (1) and (2) is 98 and 3%, respectively.

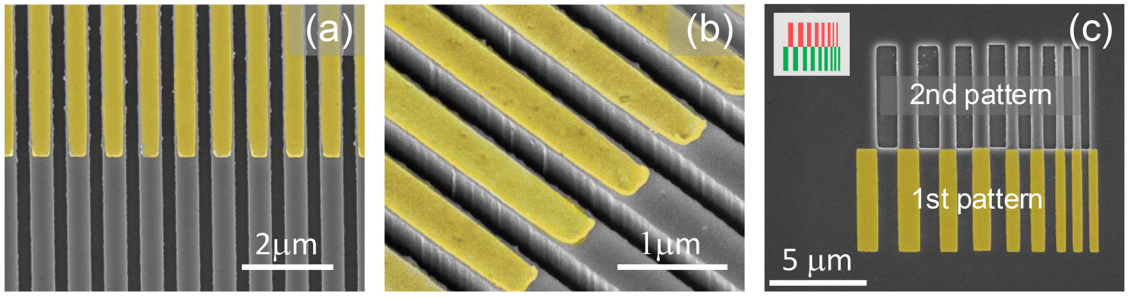

Figure 3: Fabricated MetalMHCG structures.
(a) Top-view, (b) Oblique-view false-colored SEM images. (c) Investigation of the alignment quality of the overlaid markers. The inset in (c) depicts the layout of the first and second markers.

SEM images of the fabricated metalMHCG revealed very close to rectangular cross-sections and geometrical parameters that matched very well to the design parameters: $L = 793 \pm 3$ nm; $a = 509 \pm 9$ nm; $H = 397 \pm 16$ nm. The widths of the gold stripes on top of the GaSb stripes were $a_m = 427 \pm 6$ nm in the metalMHCG configuration. The metal stripes were made slightly narrower than the semiconductor stripes to anticipate alignment errors originating from the first and second patterning. However, as became evident from our numerical simulation (Supplementary Figure S1), there was little difference between the transmission spectra of the metalMHCG configuration and the ideal case of metal and semiconductor stripes of equal widths. In both cases, the maximal value of transmission remained nearly unchanged and blueshifted by 5%.

The spectral responses were experimentally characterized using a microscope integrated with infrared light sources from Fourier-transform infrared spectrometer system (described in Supplementary Material S2). The sample was slightly tilted off-normal to avoid unwanted spectral fringes caused by multiple reflections within the sample and among the optical components. Our main results are summarized in Figure 4(a), which shows the experimental and calculated transmission spectra of the metalMHCG. The transmission of the metalMHCG (T) was normalized with the transmission through an unpatterned GaSb layer

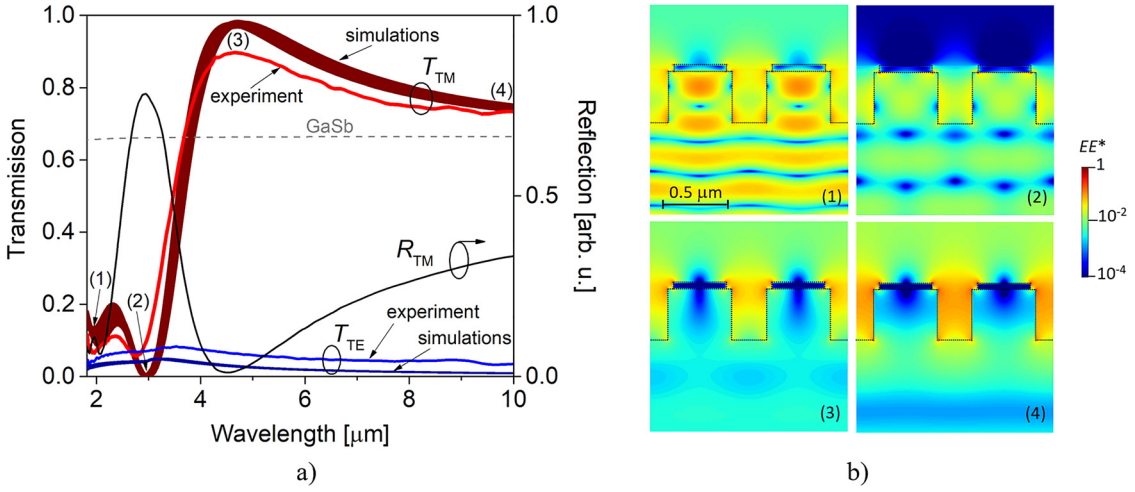

Figure 4: (a) Experimental spectra of transmittance for the metalMHCG illuminated by TM (red) and TE (blue) polarizations; simulated spectra of transmittance for TM (dark red) and TE (dark blue) polarizations, multiple, overlapping lines represent combinations of errors in determining the metalMHCG parameters; gray dashed line represents Fresnel transmission through the plane interface between the GaSb and air, based on GaSb refractive index dispersion [31]. Numbers (1)–(4) indicate wavelengths and corresponding light distributions illustrated in (b); the black line and right axis represent the experimental spectrum of power reflectance determined in arbitrary units for TM polarization. (b) Distributions of optical field intensity within a metalMHCG illuminated by TM polarizations of various wavelengths.

on the same sample. The value of Fresnel transmission through the uniform layer was aligned with the theoretical value indicated by a gray dashed line in the figure. The comparison of theoretical and experimental Fresnel transmission provides Figure S1 in Supplementary Materials. The theoretical dependence is determined for absorption-free material. Therefore in the range $\lambda < 4$ μm experimental Fresnel transmission deviates from the theoretical one due to the presence of interband absorption that increases with the decrease in the wavelength. The experimental TM-polarized transmission through the metalMHCG revealed a prominent maximum of $T \cong 90\%$ at $\lambda = 4.64$ μm, as indicated by the red solid line in the figure. This is the highest transmission experimentally reported for a 1D metal grating structure deposited on a high refractive index semiconductor substrate.

The broadband high transmission ($75\% < T < 90\%$), which exceeds that of the Fresnel transmission of bare GaSb ($T \cong 66\%$), was observed in a spectral range from $\lambda = 3.68$ μm to the long-wavelength limit of the measurement setup. The dark red lines represent simulated spectra for possible nonidealities in the geometrical parameters (i.e., L, a, a_m, H). Owing to the excellent agreement between the simulated and measured spectra, the discrepancy between the simulated and experimental spectra cannot be attributed to the deviations in the geometrical parameters, nor to the slight tilting of the sample to prevent unwanted multiple reflections.

We also simulated the effect of incidence angles on the transmission spectra (at $\lambda = 4.64$ μm), to take into account the reflection-type objective lens used in the characterization, as shown in the Supplementary materials (Figure S4). The reflection-type objective lens blocks the normal incidence part of the illumination, and according to its specification allows incidence angles (θ) from $\theta = 15°$ to 30° (corresponding to a lens numerical aperture of 0.5). The transmission varies by 1% as the incidence angle is increased from $\theta = 0°$ to 30°, indicating that the incidence angle is not the main factor causing the discrepancy between the measurement and the simulation. We hypothesize that the 8% lower transmission in the experimental transmittance is attributable to the sidewall corrugations, which are visible in Figure 2(a). It is well known that dry etching causes hard mask materials to be sputtered and redeposited onto a sample, creating what is commonly termed a 'micromasking artifact'. We believe that the corrugations are the result of micromasking near the sidewall of the GaSb stripes. Such micromasking incidences can be reduced by further optimization of the dry etching process. High transmission at $\lambda = 4.64$ μm was additionally confirmed by reflectance measurements (black line), revealing near-zero reflection. This indicates an elimination of the Fresnel reflection and reflection by the metal as predicted by the simulations [33]. The reflection measurements were normalized with respect to reflection from a 50 nm thick

gold pad on the same sample, and hence together with the transmission and possible absorption cannot be summed to 1.

The experimental transmittance decreased abruptly to a level not exceeding 20% at $\lambda < 3.5$ μm, which is a symptom of interference between the incident plane wave and the grating modes. This interaction was verified by calculating the light distribution in the metalMHCG, as illustrated in Figure 4(b) for the two transmission minima indicated by (1) and (2) in Figure 4(a). At these minima, light significantly cumulates in the semiconductor stripes, which is a fingerprint of leaky grating modes present in this configuration [33] but absent at the wavelengths corresponding to the maximum of transmission and to the experimental limit of 10 μm (Figure 4(b), (3) and (4)). The experimental reflectance followed the theoretical trend, with the increased reflection of shorter wavelengths. However, it is shadowed by the increased absorption of GaSb in this spectral range [40]. The experimental transmission spectrum for TE polarization (blue line) shows nearly total elimination of light transmission. This behavior is also in excellent agreement with the simulations (dark blue lines) representing the spectra of metalMHCGs, assuming possible nonidealities in the geometrical parameters as in the case of TM transmission. Simulations show that when the TE-polarized light interacts with the grating, it is funneled by the grating stripes and reflected by the metal, as Figure 2(d) illustrates. In the experiment, the ratio of TM to TE transmission at $\lambda = 4.64$ mm was 15 and increased to 21 at a wavelength of 10 mm.

Based on the geometrical parameters of the gold stripes extracted from SEM images, sheet resistance can be estimated using the formula:

$$R_s = \frac{\rho L}{H_m (L - a_m)}, \tag{1}$$

where ρ is the electrical resistivity of the gold stripes. To consider gold stripes of nanoscale cross-sectional dimensions, it is necessary to take into account conductivity-size effects that deteriorate the electrical resistivity of bulk gold ($2.2{\cdot}10^{-8}$ Ωm)—as employed in [41]. For the geometrical parameters of the metal stripes used in the experiment ($L = 793 \pm 3$ nm, $H_m = 50$ nm, and $a_m = 427 \pm 6$ nm), this gives resistivity at the level of $5{\cdot}10^{-8}$ Ωm and sheet resistance of 2.21 ± 0.01 ΩSq^{-1}. To verify the numerical analysis, we performed experimental verification of the sheet resistance of metalMHCG. Using silver conductive paste on both lateral borders of the metalMHCG that footprint is 100 × 100 μm we performed characterization of current flow along the metal stripes that is detailed in Supplementary Materials S3. The measured resistance of the metalMHCG was at the level of $130\ 10^{-8}$ Ωm that enables sheet resistance of 26 ΩSq^{-1}. The level of resistivity that we determined corresponds well to resistivities of the Au stripes of similar cross-section dimensions reported in the past [42, 43]. A significantly higher value of measured resistivity with respect to theoretical resistivity of nano size Au wires is mainly caused by grain boundaries impeding the electron transport. Nevertheless measured metalMHCG sheet resistance is 10 times lower than the sheet resistance of the ITO layer enabling 90% transmission when implemented on low refractive index glass or polymer [15, 44]. Perfection of methods of Au nanowire deposition enabling higher smoothness of the metal boundaries reduces their resistivity to near-bulk level [45] of $2.26{\cdot}10^{-8}$ Ωm [46] and hence near 1 ΩSq^{-1} sheet resistance.

3 Conclusions

In conclusion, this paper presents the first experimental demonstration of a monolithic high contrast grating integrated with metal stripes, enabling maximum 90% transmission of polarized light. The structure has a broadband high transmittance range ($75\% < T < 90\%$), exceeding Fresnel transmittance in the range from $\lambda = 4$ to 10 μm, limited by the capabilities of the experimental setup. The high transmission of the metalMHCG configuration is enabled by the creation of low-quality factor resonance in the air gaps between the grating stripes and elimination of light cumulation at the interface between the metal and semiconductor stripes. Both effects strongly reduce light absorption and reflection by the metal stripes, which is evidenced by the reflection spectrum of the metalMHCG. The metalMHCG reveals strong polarization selectivity and sheet resistance at the level of 26 ΩSq^{-1} that can be further reduced to the level of a few ΩSq^{-1}. All experimental results presented in this paper are in excellent agreement with theory, which predicts above 98% transmission for the tested configuration. Such high transmission could be achieved experimentally by perfecting the process of grating fabrication. The reduction in light absorption predicted by the theory could enable radically low sheet resistance of 0.1 ΩSq^{-1} by the possible implementation in the metalMHCG structure of very thick metal stripes [33].

At a more general level, this work opens up a new avenue for optically transparent and electrically highly conductive structures that can be monolithically integrated with a multitude of materials used in optoelectronics, particularly with high refractive index semiconductors, enabling the elimination of Fresnel reflection. The

metalMHCG facilitates light transmission in spectral ranges from ultra-violet to infrared [33]. The metalMHCG not only enables lateral transport of electrons but also can be used as an electric contact for current injection into a semiconductor since the metal can be implemented directly on a semiconductor.

Author contributions: All the authors have accepted responsibility for the entire content of this submitted manuscript and approved submission. The authors acknowledge Nanyang Nanofabrication Centre (N2FC) for facilitating the device fabrication.

Research funding: This work is supported by A*STAR (SERC 1720700038 and A1883c0002), Singapore, Narodowe Centrum Badań i Rozwoju (NCBR) (HybNanoSens no. DZP/POL-SINIV/283/2017) and Narodowe Centrum Nauki (OPUS 018/29/B/ST7/01927).

Conflict of interest statement: The authors declare no conflicts of interest regarding this article.

References

[1] E. Fortunato, D. Ginley, H. Hosono, and D. C. Pain, "Transparent conducting oxides for photovoltaics," *Mater. Res. Soc. Bull.*, vol. 32, pp. 242–247, 2007.

[2] D. J. Lipomi, M. Vosgueritchian, B. C.-K. Tee, et al., "Skin-like pressure and strain sensors based on transparency elastic films of carbon nanotubes," *Nat. Nanotechnol.*, vol. 6, pp. 788–792, 2011.

[3] H. Peng, W. Dang, J. Cao, et al., "Topological insulator nanostructures for near-infrared transparent flexible electrodes," *Nat. Chem.*, vol. 4, pp. 281–286, 2012.

[4] A. Kumar and C. W. Zhou, "The race to replace tin-doped indium oxide: which material will win?" *ACS Nano*, vol. 4, pp. 11–14, 2010.

[5] Z. Wu, Z. Chen, X. Du, et al., "Transparent, conductive carbon nanotube films," *Science*, vol. 305, pp. 1273–1276, 2004.

[6] M. Zhang, S. L. Fang, A. A. Zakhidov, et al., "Strong, transparent, multifunctional, carbon nanotube sheets," *Science*, vol. 309, pp. 1215–1219, 2005.

[7] M. G. Kang and L. J. Guo, "Nanoimprinted semitransparent metal electrodes and their application in organic light-emitting diodes," *Adv. Mater.*, vol. 19, pp. 1391–1396, 2007.

[8] S. R. Forrest, "The path to ubiquitous and low-cost organic electronic appliances on plastic," *Nature*, vol. 428, pp. 911–918, 2004.

[9] G. Liang, Z. Liu, F. Mo, et al., "Self-healable electroluminescent devices," *Light Sci. Appl.*, vol. 7, p. 102, 2018.

[10] T. C. Lu, C. C. Kao, H. C. Kuo, G. S. Huang, and S. C. Wang, "CW lasing of current injection blue GaN-based vertical cavity surface emitting laser," *Appl. Phys. Lett.*, vol. 92, p. 141102, 2008.

[11] T.-C. Lu, S.-W. Chen, T.-T. Wu, et al., "Continuous wave operation of current injected GaN vertical cavity surface emitting lasers at room temperature," *Appl. Phys. Lett.*, vol. 97, p. 071114, 2010.

[12] T. A. König, P. A. Ledin, J. Kerszulis, et al., "Electrically tunable plasmonic behavior of nanocube-polymer nanomaterials induced by a redox-active electrochromic polymer," *ACS Nano*, vol. 8, pp. 6182–6192, 2014.

[13] Y.-J. Moon, S.-W. Kim, H. S. An, et al., "Engineered unidirectional scattering in metal wire networks for ultrahigh glass-like transparency," *ACS Photonics*, vol. 5, pp. 4270–4276, 2018.

[14] E. J. López-Naranjo, L. J. González-Ortiz, L. M. Apátiga, E. M. Rivera-Muñoz, and A. Manzano-Ramírez, "Transparent electrodes: A review of the use of carbon-based nanomaterials," *J. Nanomater.*, vol. 2016, p. 4928365, 2016.

[15] K. Ellmer, "Past achievements and future challenges in the development of optically transparent electrodes," *Nat. Photonics*, vol. 6, pp. 809–817, 2012.

[16] J. M. Foley, S. M. Young, and J. D. Phillips, "Symmetry-protected mode coupling near normal incidence for narrow-band transmission filtering in a dielectric grating," *Phys. Rev. B*, vol. 89, p. 165111, 2014.

[17] H. Hemmati, P. Bootpakdeetam, and R. Magnusson, "Metamaterial polarizer providing principally unlimited extinction," *Opt. Lett.*, vol. 44, pp. 5630–5633, 2019.

[18] C. Maës, G. Vincent, F. González-Posada Flores, L. Cerutti, R. Haïdar, and T. Taliercio, "Infrared spectral filter based on all-semiconductor guided-mode resonance," *Opt. Lett.*, vol. 44, pp. 3090–3093, 2019.

[19] E. Hutter and J. H. Fendler, "Exploitation of localized surface plasmon resonance," *Adv. Mater.*, vol. 16, pp. 1685–1706, 2004.

[20] W. L. Barnes, W. A. Murray, J. Dintinger, E. Devaux, and T. W. Ebbesen, "Surface plasmon polaritons and their role in the enhanced transmission of light through periodic arrays of subwavelength holes in a metal film," *Phys. Rev. Lett.*, vol. 92, p. 107401, 2004.

[21] K. J. Koerkamp, S. Enoch, F. B. Segerink, N. F. van Hulst, and L. Kuipers, "Strong influence of hole shape on extraordinary transmission through periodic arrays of subwavelength holes," *Phys. Rev. Lett.*, vol. 92, p. 183901, 2004.

[22] J. B. Pendry, L. Martín-Moreno, and F. J. Garcia-Vidal, "Mimicking surface plasmons with structured surfaces," *Science*, vol. 305, pp. 847–848, 2004.

[23] M. M. J. Treacy, "Dynamical diffraction in metallic optical gratings," *Appl. Phys. Lett.*, vol. 75, p. 606, 1999.

[24] J. A. Porto, F. J. Garcia-Vidal, and J. B. Pendry, "Transmission resonances on metallic gratings with very narrow slits," *Phys. Rev. Lett.*, vol. 83, p. 2845, 1999.

[25] Q. Cao and P. Lalanne, "Negative role of surface plasmons in the transmission of metallic gratings with very narrow slits," *Phys. Rev. Lett.*, vol. 88, p. 057403, 2002.

[26] J. Tong, F. Suo, J. Ma, L. Y. M. Tobing, L. Qian, and D. H. Zhang, "Surface plasmon enhanced infrared photodetection," *Opto-Electronic Adv.*, vol. 2, pp. 18002601–18002610, 2019.

[27] J. Tong, L. Y. M. Tobing, S. Qiu, D. H. Zhang, and A. G. Unil Perera, "Room temperature plasmon-enhanced InAs 0.91 Sb 0.09 -based heterojunction n-i-p mid-wave infrared photodetector," *Appl. Phys. Lett.*, vol. 113, p. 011110, 2018.

[28] L. Y. M. Tobing, L. Tjahjana, D. H. Zhang, Q. Zhang, and Q. Xiong, "Sub-100-nm sized silver split ring resonator metamaterials with fundamental magnetic resonance in the middle visible spectrum," *Adv. Opt. Mater.*, vol. 2, pp. 280–285, 2014.
[29] A. A. Darweesh, S. J. Bauman, D. T. Debu, and J. B. Herzog, "The role of Rayleigh-wood anomalies and surface plasmons in optical enhancement for nano-gratings," *Nanomaterials*, vol. 8, p. 809, 2018.
[30] L. Dai and C. Jiang, "Anomalous near-perfect extraordinary optical absorption on subwavelength thin metal film grating," *Opt. Express*, vol. 17, pp. 20502–20514, 2009.
[31] H. Kim, "Metallic triangular pillar grating arrays for high transmission polarizers for air:glass interfaces," *Jpn. J. Appl. Phys.*, vol. 58, p. 042001, 2019.
[32] C. Stelling, C. R. Singh, M. Karg, T. A. F. König, M. Thelakkat, and M. Retsch, "Plasmonic nanomeshes: their ambivalent role as transparent electrodes in organic solar cells," *Sci. Rep.*, vol. 7, p. 42530, 2017.
[33] T. Czyszanowski, A. K. Sokół, M. Dems, and M. Wasiak, "Transparent electrode employing deep-subwavelength monolithic high-contrast grating integrated with metal," *Opt. Express*, vol. 28, pp. 28383–28398, 2020.
[34] J. Piprek, *Semiconductor Optoelectronic Devices Introduction to Physics and Simulation*, San Diego, Academic Press, 2003.
[35] M. Grabherr, M. Miller, R. Jager, et al., "High-power VCSELs: single devices and densely packed 2-D-arrays," *IEEE J. Sel. Top. Quant. Electron.*, vol. 5, pp. 495–502, 1999.
[36] M. Dems, "Modelling of high-contrast grating mirrors. The impact of imperfections on their performance in VCSELs," *Opto-Electron. Rev.*, vol. 19, pp. 340–345, 2011.
[37] M. Wasiak, M. Motyka, T. Smołka, J. Ratajczak, and A. Jasik, "Absorption and dispersion in undoped epitaxial GaSb layer," *Mater. Res. Express*, vol. 5, p. 025907, 2018.
[38] R. L. Olmon, B. Slovick, T. W. Johnson, et al., "Optical dielectric function of gold," *Phys. Rev. B*, vol. 86, p. 235147, 2012.
[39] P. Qiao, W. Yang, and C. J. Chang-Hasnain, "Recent advances in high-contrast metastructures, metasurfaces, and photonic crystals," *Adv. Opt. Photonics*, vol. 10, pp. 180–245, 2018.
[40] R. Ferrini, M. Patrini, and S. Franchi, "Optical functions from 0.02 to 6 eV of $Al_xGa_{1-x}Sb$/GaSb epitaxial layers," *J. Appl. Phys.*, vol. 84, pp. 4517–4524, 1998.
[41] A. K. Sokół and T. Czyszanowski, "Nearly perfect transmission of unpolarized infrared radiation through a one-dimensional metal grating embedded in a monolithic high-contrast grating," *Opt. Express*, vol. 28, pp. 38857–38866, 2020.
[42] S. Valizadeh, M. Abid, F. Hernández-Ramírez, A. Romano Rodríguez, K. Hjort, and J. Å. Schweitz, "Template synthesis and forming electrical contacts to single Au nanowires by focused ion beam techniques," *Nanotechnology*, vol. 17, p. 1134, 2006.
[43] J. H. Song, Y. Y. Wu, B. Messer, H. Kind, and P. D. Yang, "Metal nanowire formation using Mo_3Se_3- as reducing and sacrificing templates," *J. Am. Chem. Soc.*, vol. 123, pp. 10397–10398, 2001.
[44] *Product information of Biotain Crystal* [online]. Avaliabe at http://www.crystal-material.com/Substrate-Materials/ITO-coated-glass-conductive.html. [accessed: Sep. 19, 2021].
[45] K. Critchley, B. P. Khanal, M. Ł. Górzny, et al., "Near-bulk conductivity of gold nanowires as nanoscale interconnects and the role of atomically smooth interface," *Adv. Mater.*, vol. 22, pp. 2338–2342, 2010.
[46] Y. Peng, T. Cullis, and B. Inkson, "Accurate electrical testing of individual gold nanowires by in situ scanning electron microscope nanomanipulators. *Appl. Phys. Lett.*, vol. 93, p. 183112, 2008.

Supplementary Material: The online version of this article offers supplementary material (https://doi.org/10.1515/nanoph-2021-0286).